Primljen / Received: 23.7.2019.
Ispravljen / Corrected: 31.10.2019.
Prihvaćen / Accepted: 10.5.2020.
Dostupno online / Available online: 10.6.2022.

Seismic behaviour of composite shear wall with steel reinforced concrete frame and embedded perforated-steel plate

Authors:

Zhongyi Zhou, PhD. CE
China Earthquake Administration
Key Laboratory of Earthquake Engineering and Vibration, Institute of Engineering Mechanics
zzyhui@163.com

Prof. **Wanlin Cao**, PhD. CE
Beijing University of Technology, China
Faculty of Civil Engineering
wlcao@bjut.edu.cn

Yan Liu, PhD. CE
North China University of Science and Technology, China
Faculty of Arhhitecture
liuyan66166@163.com

Jianhua Li, PhD. CE
Huzhou Vocational and Technical College, China
Institute of Civil Engineering
xjbnljh@126.com
Corresponding autho

Research Paper

Zhongyi Zhou, Wanlin Cao, Yan Liu, Jianhua Li

Seismic behaviour of composite shear wall with steel reinforced concrete frame and embedded perforated-steel plate

Experiments are conducted on five shear wall specimens of varying design and structural measures in order to investigate seismic behaviour of a composite shear wall with the steel-reinforced concrete frame and an embedded perforated-steel plate. In addition, low-cyclic load is applied on test specimens that have a shear span ratio of 1.5. Using the experimental data, the bearing capacity, stiffness, ductility, hysteretic energy, and failure characteristics of five specimens are analysed. The results show that the composite shear wall (CSW) with the steel reinforced concrete frame (SRCF) and embedded steel plate (ESP) has higher bearing capacity, better ductility, slower degradation of stiffness, and higher energy dissipation capacity, as compared to an ordinary reinforced concrete shear wall. Moreover, its seismic behaviour can be improved by using the ESP of an appropriate thickness. For the ESPs of identical thickness, the results show that the specimen that uses steel ties exhibits better seismic behaviour than those using welding studs. Finally, a computing model that can calculate the bearing capacity of the CSWs is developed. A comparison of calculated and measured results shows that the results are close to each other.

Key words:
steel reinforced concrete frame, embedded steel plate, composite shear wall, seismic behaviour, bearing capacity calculation

Prethodno priopćenje

Zhongyi Zhou, Wanlin Cao, Yan Liu, Jianhua Li

Seizmičko ponašanje spregnutih posmičnih stijena s AB okvirom ojačanim čelikom i ugrađenom perforiranom čeličnom pločom

U radu se ispituje pet uzoraka posmičnih stijena raznih dimenzijskih i konstrukcijskih karakteristika kako bi se istražilo seizmičko ponašanje spregnute posmične stijene s armiranobetonskim okvirom ojačanim čelikom i ugrađenom perforiranom čeličnom pločom. Osim toga, niskociklično opterećenje se nanosi na uzorke s koeficijentom posmične zone od 1,5. Eksperimentalni podaci koriste se za analizu nosivosti, krutosti, duktilnosti, histerezne energije i karakteristika otkazivanja spomenutih uzoraka. Rezultati pokazuju da se spregnuta posmična stijena s armiranobetonskim okvirom ojačanim čelikom i ugrađenom čeličnom pločom odlikuje većom nosivošću, boljom duktilnošću, sporijim padom krutosti te većom sposobnošću rasapa energije u usporedbi s običnim armiranobetonskim posmičnim zidom. Osim toga, primjenom ugrađenih čeličnih ploča odgovarajuće debljine poboljšava se i seizmičko ponašanje spregnutih posmičnih stijena. Analizom čeličnih ploča iste debljine utvrđeno je da se uzorci s čeličnim vezicama seizmički bolje ponašaju od uzoraka sa zavarenim svornjacima. U završnom je dijelu razvijen računalni model za izračunavanje nosivosti CSW-a. Usporedba pokazuje dobru podudarnost rezultata proračuna i rezultata dobivenih mjerenjem.

Ključne riječi:
armiranobetonski okvir ojačan čelikom, ugrađena čelična ploča, spregnuta posmična stijena, seizmičko ponašanje, proračun nosivosti

1. Introduction

In significant seismic hazard areas, steel plate shear walls (SPSWs) constitute an important lateral load supporting system for high- and super-high rise buildings due to their initial high stiffness, high deformation ability, good plasticity, and stable hysteretic properties [1-4]. However, in the case of traditional unrestrained SPSWs, horizontal load can easily lead to the out-of-plane buckling, fast degradation of stiffness, and serious pinching of hysteretic loop. These occurrences can reduce the energy dissipation capacity of SPSWs. Some researchers have conducted experimental studies and theoretical analyses for the out-of-plane buckling of SPSWs. Chen S J examined the effects of the width-to-thickness ratio on the shear buckling of low-yield-point steel plates [5]. Elgaaly M described analytical models that are capable of accurately predicting wall behaviour in the post-buckling domain under monotonic and cyclic loads [6].

Tsai K C presented experimental and analytical results of four large-scale steel panel shear wall (SPSW) frames tested in the National Centre for Research on Earthquake Engineering (NCREE). The test confirmed that the proposed restrainers can effectively reduce the magnitude of the buckling sound and the out-of-plane buckling of SPSWs subjected to large inter-story drifts [7].

Guo et al. studied a buckling-restrained SPSW, and investigated its elastic behaviour and the concrete slab restrained stiffness [8]. Based on the low-cyclic load experiments, Lu et al. studied characteristics and modelled recovering forces of the steel plated reinforced concrete shear walls, and developed equations for calculating the shear bearing capacity [9].

Sun et al. investigated the shear failure modes, ultimate bearing capacity, and ductility of steel plate-concrete CSWs with various types of connections. They also developed equations for computing shear strength of the CSWs with restraining conditions at the shear section [10]. Using the quasi-static test, Jiang et al. conducted studies on CSWs with concealed columns installed at the two sides and a centrally embedded steel plate. They also analysed the bearing capacity, hysteretic behaviour, deformability, and failure mechanism of each specimen. Furthermore, the experimental studies and theoretical analyses of the overall seismic behaviour of CSWs with concrete filled steel tube columns and ESP has been systematically conducted [11-16]. Tian, S. M. studied the design method involving shear bolt for a steel plate concrete shear wall [17].

The above-mentioned studies focused on the overall seismic performance of embedded steel reinforced concrete CSWs. They seldom pay attention to the influence of the plate thickness and steel plate-concrete connecting structure on the seismic behaviour of CSWs with SRCF and ESP. Therefore, a CSW comprising a SRCF, an EPSP and concrete is developed in this study. In the wall, reinforcement is placed transversely and longitudinally on both sides of the embedded steel plate. Through the holes in the plate, using steel ties, the reinforcing mattresses are connected to the sides.

Thus, the CSW takes advantage of both the SRCF and the SPSW. On the one hand, the holes on the plate can be used to adjust the stiffness ratio of the ESP and the frame so as to avoid the pinching of steel wall members, resulting in a high safety margin. On the other hand, the steel ties can connect the two reinforced nets via the holes so as to enhance structural integrity. Subsequently, experiments are conducted on five specimens subjected to low-cyclic loading. Based on the experimental results, the effects of various design parameters and structural measures with different types of connections on the seismic behaviour of the CSWs with the SRCF and ESP is systematically analysed. Hence, the results of the analyses can provide technical support for this type of structures in engineering practice.

2. Experiments

2.1. Specimen design

Designed to a scale of 1:5, the five specimens have identical geometric dimensions. They are 100 mm thick and 1810 mm high, with a total section height of 740 mm in which the clear height of the wall is 460 mm. The specimens are divided into three groups. In the first group, there are three specimens of CSWs with the SRCF and EPSP (shear wall with holes hidden in the frame of steel concrete section). The thickness of EPSPs is 2 mm (specimen SPSW-1), 4 mm (specimen SPSW-2) and 6 mm (specimen SPSW-3).

Using steel ties, the EPSPs are connected to the outer-packed concrete through the following steps. 10 mm diameter holes are first punched through the steel plate. Then, using steel ties through the holes, the reinforcing mattresses are fixed to both sides of the plate. The steel ties which are iron wire Ø12 are fixed at the spacing corresponding to that of the holes. Thus, the spacing of the ties is 120 mm for the upper half of the plate, and 80 mm for the lower half of the plate. In the second group, there is only one CSW specimen with the SRCF and ESP (specimen SPSW-4).

The 4 mm thick ESP is anchored to the reinforced concrete using studs which were welded on to the plate. The studs which are M3 bolts are fixed at a spacing of 40 mm. There are ordinary steel nets at the outside of the studs. In the third group, there is also one CSW specimen with the SRCF and ordinary reinforced concrete (specimen RCSW-5) [18]. Geometric dimensions and assembled reinforcement of the five specimens are shown in Figure 1 and Figure 2.

Table 1. Mechanical properties of reinforcement and steel products used in the tests

Steel products	Yield strength [GPa]	Ultimate strength [MPa]	Ductility [%]	Elastic modulus [GPa]
2 mm-thick steel plate	221.5	359.7	27.3	206
4 mm-thick steel plate	273.8	406.3	23.4	203
6 mm-thick steel plate	278.2	405.5	24.4	209
H-shape steel	315.0	450.0	31.5	191
Ø6 reinforcement	536.0	591.0	30.0	177
Ø3 galvanized steel wire	206.5	241.5	11.5	196
Ø4 galvanized steel wire	343.5	390.0	20.7	196
Ø4 cold-drawn reinforcement	669.0	836.0	7.5	206

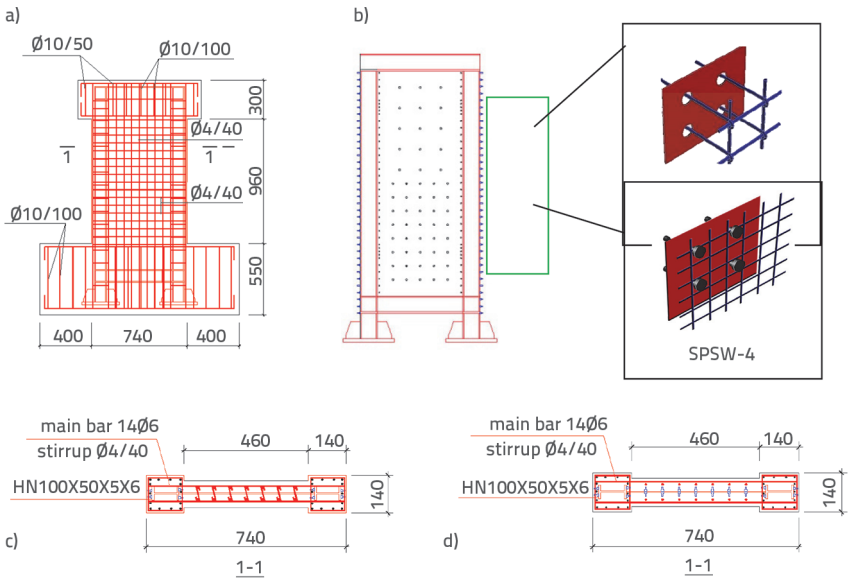

Figure 1. Display samples SPSW-1, SPSW-2, SPSW-3 and SPSW-4: a) Geometric dimensions and assembled reinforcement; b) Embedded steel plate; c) 1-1 profile of SPSW-1, SPSW-2 and SPSW-3; d) 1-1 profile of SPSW-4

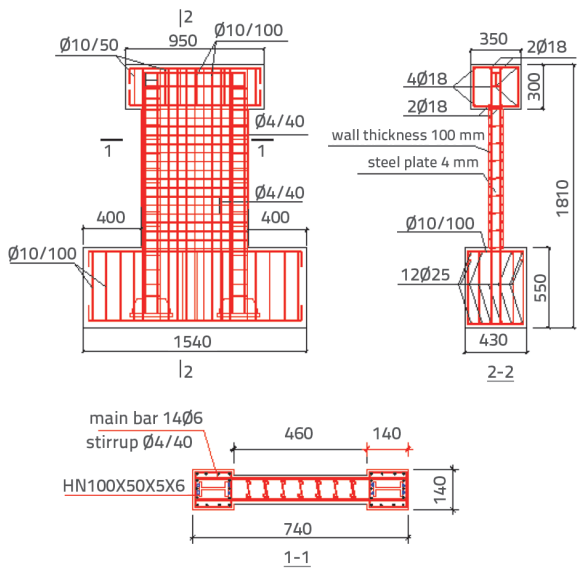

Figure 2. Geometric dimensions and assembled reinforcement of specimens RCSW-5

2.2. Material properties

The measured compressive strength of the concrete cubes of specimens SPSW-1 and SPSW-4 is 46.7 MPa with an elastic modulus of 31.3 GPa. The measured compressive strength of the concrete cubes of specimens SPSW-2, SPSW-3 and RCSW-5 is 48.1 MPa with an elastic modulus of 32.8 GPa. Mechanical properties of the reinforcement and steel products used in the tests are shown in Table 1.

2.3. Loading during experiments

Figure 3 shows a photograph of the loading setup in the experiment. The experiments were conducted under the force-displacement combination control, i.e., load control before the yield of the specimens and displacement control after the yield of the specimens. The horizontal cycled load was applied by a hydraulic actuator, and the vertical load was applied by hydraulic jacks. During the elastic period, the incremental quantity of horizontal cycled load was 20 kN and was set to be recycled once at each grade. For each level of loading, the cyclic loading included a positive load and a negative load. As the specimen came into plastic stage, the incremental quantity was up to yield displacement Δy or 0.5 times the yield displacement.

During the experiment, a constant vertical load of 870 kN was first applied on the specimens, with an axial compression ratio of 0.45. Then low-cyclic lateral loads were applied at various levels.

The forces, displacements, and strains of the specimens were recorded using the IMP data acquisition system. The load-displacement hysteretic curves were also automatically plotted by the system. The cracks on the specimens were manually observed and depicted.

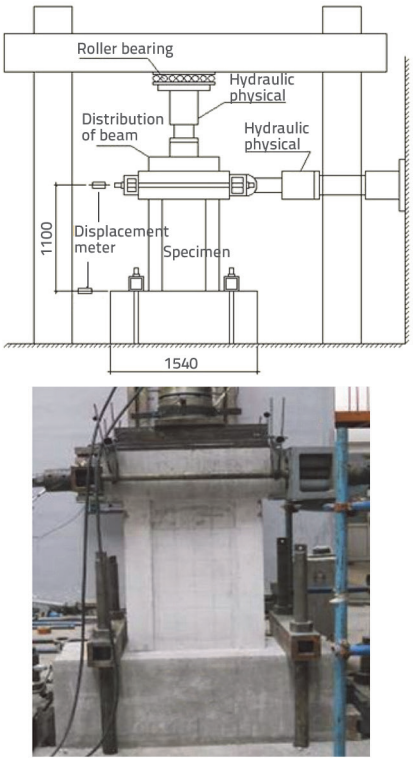

Figure 3. Loading setup in the experiment: test scheme (above), test sample display (below)

3. Results and discussion

3.1. Test results

Figure 4 shows failure modes of the five specimens. The following can be observed:

1. As compared to the reinforced concrete shear wall (RCSW-5), the cracks in the CSWs with the SRCF and the ESP (SPSW-1, 2, 3 and 4) are diagonal, more uniformly distributed, and show a relatively small development. There are denser and larger-area cracks in the specimen (SPSW-2) with steel ties as the shearing connector, as compared to the one with welding studs.
2. For all five specimens, the compression failure started at the bottom of the concrete side columns on the outside. Generally, vertical cracks first started to appear on the outside of the side columns, which was followed by the flaking off of the outer concrete. The longitudinal reinforcement then started to bend, followed by the buckling of steel flanges and the spreading of cracks. Finally, the entire cross-section of concrete crushed resulting in failure of the specimen.
3. As the thickness of ESP increases, the cracks tend to move to the lower and middle segments of the wall. The crushed portion of concrete gradually extended upwards to about 1/3 of the column height (Figures 4 (a) ~ (c)). As such, the middle segments of the columns were subjected to additional load through tensile forces generated by the ESP. This adversely affected the bearing capacities of the ESP.
4. The cracks in Figure 4(b) are slightly denser and more evenly distributed as compared to those in Figure 4(d), even though they follow a similar distributing rule.

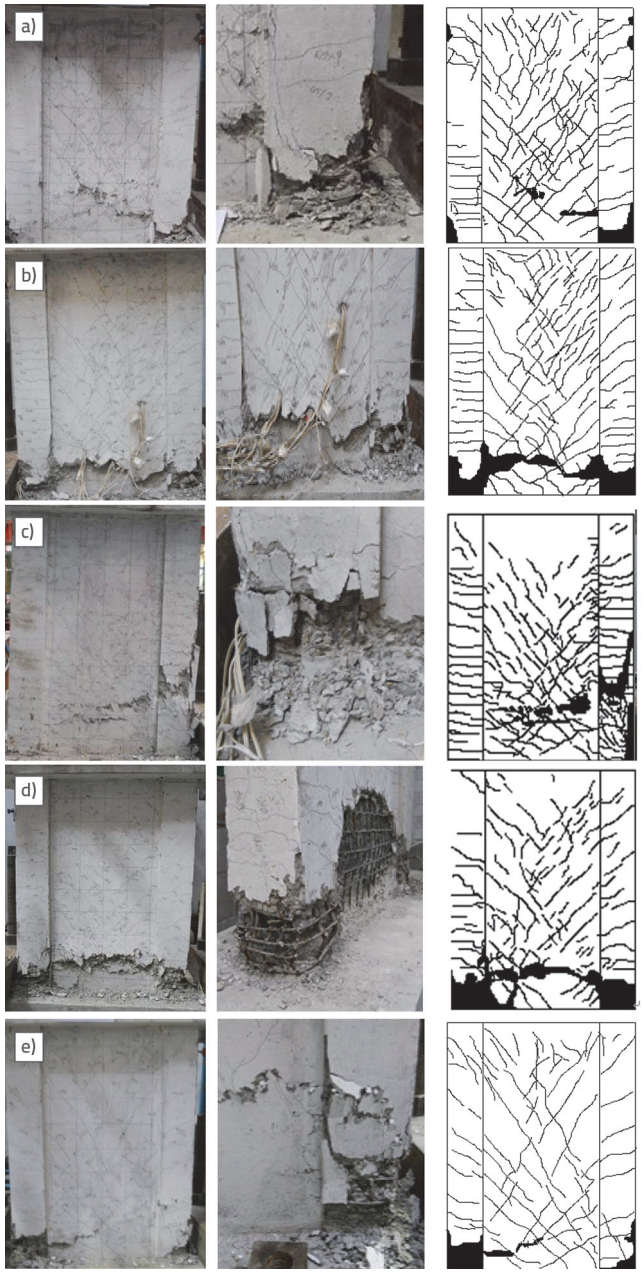

Figure 4. Failure modes of the five specimens: a) SPSW-1; b) SPSW-2; c) SPSW-3; d) SPSW-4; e) SPSW-5

3.2. Bearing capacity

Table 2 shows the measured cracking load, apparent yield load, and characteristic load of the five specimens. As compared to those of RCSW-5, for SPSW-1, SPSW-2, SPSW-

Table 2. Measured cracking load, apparent yield load, ultimate load of five specimens*

Specimens	Cracking loads, F_c [kN]	F_c Relative magnitude	Yield load, F_y [kN]	F_y Relative magnitude	Ultimate load, F_u [kN]	F_u Relative magnitude
SPSW-1	150.5	1.03	469.2	1.33	706.5	1.23
SPSW-2	201.9	1.38	604.0	1.72	782.2	1.36
SPSW-3	155.1	1.06	624.4	1.77	772.5	1.34
SPSW-4	206.4	1.41	552.9	1.57	763.2	1.33
RCSW-5	146.7	1.00	352.0	1.00	574.6	1.00

F_c - the cracking load, F_y - the apparent yield load, F_u - the ultimate load and μ_{yu} - F_y / F_u is the yield ratio (F_y / F_u).

Table 3. Representative energy dissipation of the five specimens*

Specimen	**EP** [kNmm]	**Δ**
SPSW-1	27463	1.78
SPSW-2	35510	2.30
SPSW-3	22186	1.44
SPSW-4	32768	2.12
RCSW-5	15426	1.00

EP is the representative energy dissipation and Δ is the relative representative energy dissipation of the specimen. i.e., the ratio of the representative energy dissipation of the CSW with the SRCF and the ESP to the CSW with the SRCF and the ordinary reinforced concrete.

3 and SPSW-4, the cracking loads are respectively by 3 %, 38 %, 6 %, and 41 % higher, the yield loads are respectively by 33 %, 72 %, 77 %, and 57 % higher, and the ultimate loads are respectively by 23 %, 36 %, 34 %, and 33 % higher. Moreover, for the four CSW specimens with the SRCF and ESP, the SPSW-2 has the highest ultimate bearing capacity. This shows that the ESP thickness corresponds to bearing capacity of the CSW, although it is not proportional to the plate thickness. Thus, a plate of an appropriate thickness can improve the seismic behaviour of the CSWs. In addition, as a shear wall specimen with the EPSP, SPSW-2 has a slightly higher ultimate bearing capacity as compared to that of SPSW-4 with ESP, which had the studs welded on. Hence, the structural measure using steel ties in the EPSP is stronger than those using welding studs.

Cracking load refers to the load value corresponding to the load-displacement curve (skeleton curve) when a batch of uniform and small cracks first appears in a certain range of walls, and the curvature of skeleton curve has a certain sudden change.

3.3. Hysteresis and energy dissipation

Figure 5 shows hysteretic curves of the five specimens. As compared to that of RSW-5, the hysteretic loops of SPSW-1, SPSW-2, SPSW-3 and SPSW-4 are broader and cover larger areas. This is an indication that the CSWs with ESP have a higher energy dissipation capacity. Additionally, the hysteretic loop of SPSW-2 is the broadest and covers the largest area. This is an indication that the seismic behaviour of the CSWs with the SRCF and ESP can be improved using a plate of an appropriate thickness. As compared to SPSW-4, SPSW- 2 has a slightly higher carrying capacity, a broader hysteretic loop, and a greater energy dissipation capacity. This is an indication that the specimens using steel ties in the EPSP have better seismic behaviour than the ESP using welding studs.

The representative energy dissipation of the five specimens is shown in Table 3. The area enclosed by the outer hysteretic curve is defined as the representative energy dissipation. Thus, the representative energy dissipation is only a part of the actual energy dissipation.

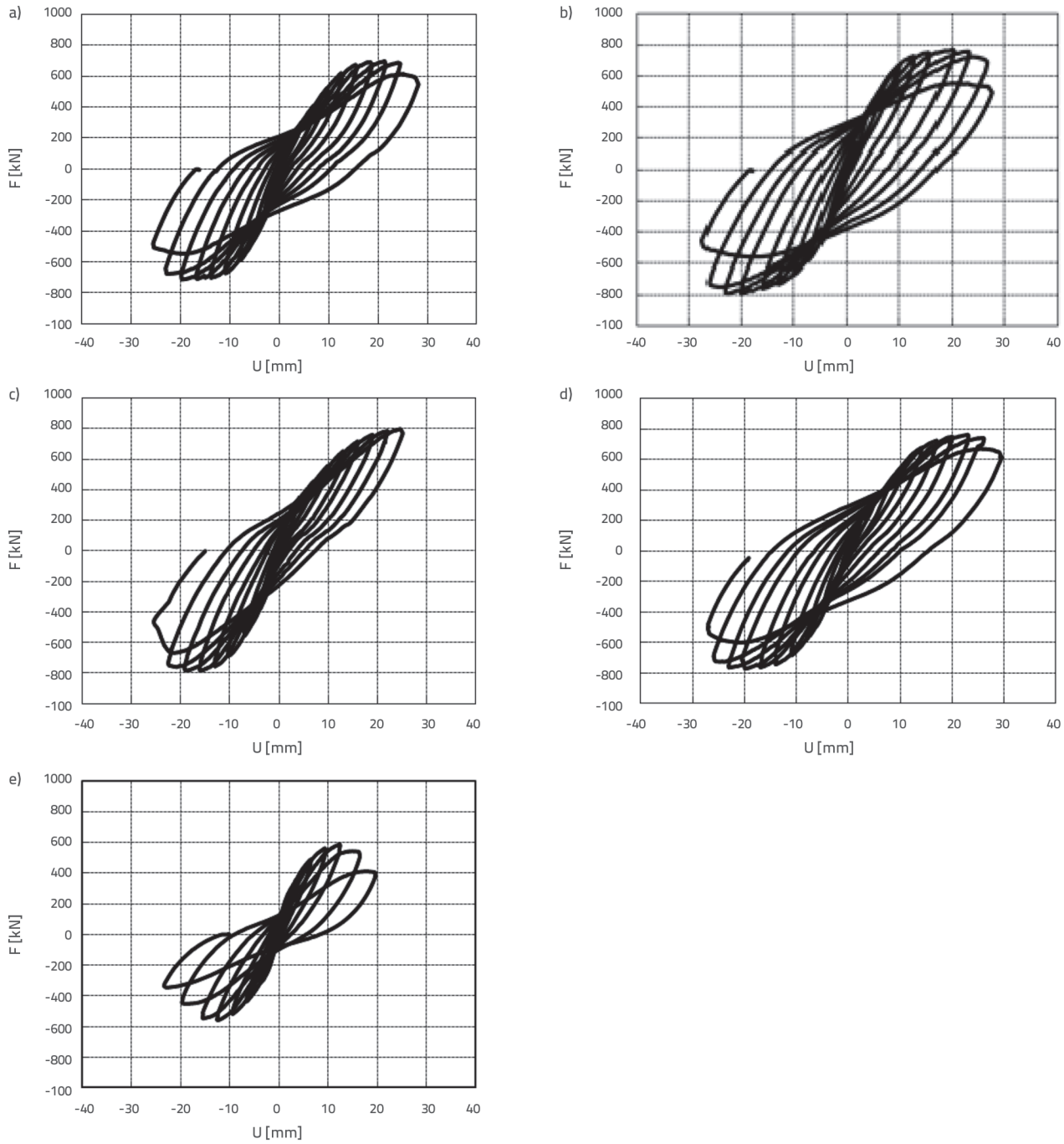

Figure 5. Hysteretic curves of the five specimens: a) SPSW-1; b) SPSW-2; c) SPSW-3; d) SPSW-4; e) SPSW-5

As shown in Table 3, the energy dissipation values of SPSW-1, SPSW-2, SPSW-3 and SPSW-4 are respectively by 78 %, 130 %, 44 % and 112 %, higher than that of RCSW-5. The specimens with the 4 mm thick plate (SPSW-2 and SPSW-4) have a larger energy dissipation capacity. Thus, the seismic behaviour of CSWs with the SRCF and the ESP can be improved by using an ESP of an appropriate thickness, although it is not positively related to the thickness. Moreover, as compared to SPSW-4, SPSW-2 has a larger energy dissipation capacity. This is an indication that the specimens using steel ties in the EPSP have better seismic behaviour than those using welding studs.

3.4. Backbone and ductility

Table 4 shows the cracking displacement, yield displacement, and ultimate displacement of the five specimens. As compared to those of RCSW-5, the cracking displacements of SPSW-1,

Table 4. Cracking displacement, yield displacement and ultimate displacement of the five specimens*

Specimen	Cracking displacement Uc [mm]	Relative value Uc	Yield displacement Uy [mm]	Relative value Uy	Maximal elastic-plastic displacement Ud [mm]	Relative value Ud	μ	Relative value μ	θ_p
SPSW-1	1.26	0.91	6.74	1.27	26.46	1.53	3.93	1.21	1/42
SPSW-2	1.57	1.14	7.28	1.37	26.96	1.55	3.70	1.13	1/41
SPSW-3	1.24	0.90	8.74	1.64	22.60	1.30	2.59	0.79	1/49
SPSW-4	1.69	1.22	7.89	1.48	25.53	1.47	3.24	0.99	1/43
RCSW-5	1.38	1.00	5.32	1.00	17.35	1.00	3.26	1.00	1/64

U_c - the cracking displacement corresponding to the cracking load Fc, U_y - the yield displacement corresponding to the yield load F_y, U_d - the maximal elastic-plastic displacement corresponding to the ultimate load dropping to 85%, θp = U_d / H - the elastic-plastic displacement angle, H - the distance from the top of the base to the centre of the loading beam, μ - the ductility coefficient (Ud / Uy).

SPSW-2, SPSW-3 and SPSW-4 are similar, the yield displacements are respectively by 27 %, 37 %, 64 %, 48 % greater, and the elastic-plastic maximal displacements are respectively by 53 %, 55 %, 30 %, 47 % greater. For the four specimens with the ESP, the ductility coefficient gradually decreases with an increase in the steel plate thickness. This is an indication that the stiffness increases, and the deformability of specimens decreases, with an increase in plate thickness. The elastic-plastic displacement angles of SPSW-1, SPSW-2 SPSW-3 and SPSW-4 are greater than 1/50, while that of RCSW-5 is 1/64, which shows that the CSWs with the SRCF and the ESP have higher ductility and elastic-plastic deformation capacity as compared to those of the ordinary reinforced concrete shear wall. As compared to SPSW-4, SPSW-2 has a higher ductility coefficient even though they have similar ultimate displacements. This shows that the structural measure using steel ties in the EPSP is stronger than those using welding studs.

Note: U at Figure 6 is the horizontal displacement of loading point at the top of specimen and F is the applied horizontal load

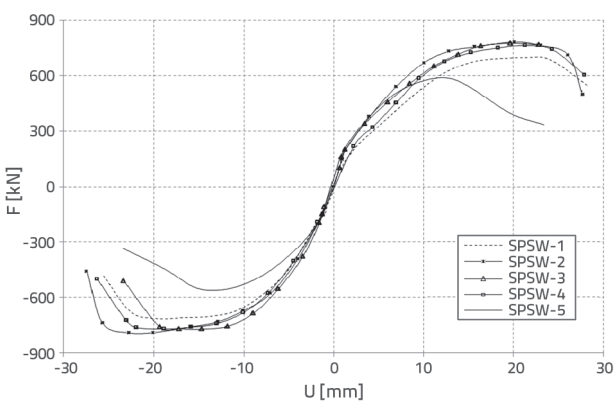

Figure 6. Backbone curve

As shown in Figure 6, the backbone curve is formed by connecting the peak point on the hysteresis curve at each cycle, which reflects the changes in the displacements of the specimen corresponding to the loading. As compared to RCSW-5, SPSW-1, SPSW-2, SPSW-3 and SPSW-4 have higher bearing capacity, lower degeneration of stiffness, larger elastic-plastic displacement, higher deformability, and significant improvement of seismic capacity. Furthermore, seismic behaviour of shearing walls can be enhanced using an appropriate plate thickness. This is demonstrated by SPSW-2 and SPSW-4, which have slightly higher bearing capacity and ductility values as compared to other specimens. The bearing capacity and ductility values of SPSW-2 are higher than those of SPSW-4. This is an indication that the specimens using steel ties in the EPSP have better seismic behaviour than the ESP using welding studs. Finally, it can be noticed (e.g., Figure 6.) that all specimen except SPSW-5 have very similar backbone curves.

3.5. Stiffness degradation

During the repeated low-cyclic loading experiments, the stiffness of the specimens gradually reduces with an increase in the number of loading cycles. As shown in Figure 7, K- θ. curve is used to depict the stiffness changing trend. It can be seen that for all the five specimens, even though their initial stiffness values are similar, their stiffness values slowly degrade resulting in large ultimate displacement angles. This is an indication that they exhibit good ductility and high seismic capability. In addition, the stiffness of the specimen increases with an increase in ESP thickness. As such, the slope of stiffness degrading curve rises, resulting in lower ductility. The specimen SPSW-2 with the ESP 4 mm in thickness exhibits a relatively flat stiffness degradation curve, i.e., the stiffness degrades slowly with a large displacement angle. This is an indication that the seismic behaviour of the shear walls can improve if a plate of an appropriate thickness is used. Note: K at Figure 7 is the secant stiffness at the peak of a hysteretic curve corresponding to the peak load within each cycle; θ is the displacement angle of the loading point under the peak load within each cycle.

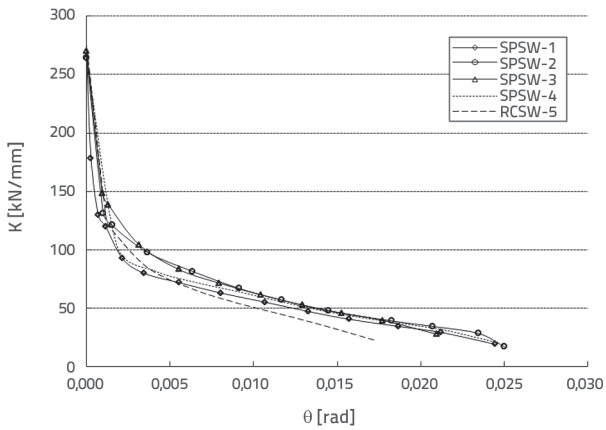

Figure 7. Stiffness degradation curves

4. Calculating bearing capacity of CSW

According to experimental results, the major mode of failure in the specimens is the bending failure, which is due to large eccentric compression. As the specimens fail due to bending, the bending moment at the bottom of columns is the most crucial. In the tension zone, as the reinforcement and the shape steel within the side column are reaching their yield stresses, most of the vertical reinforcement and the ESP in the shear wall are also reaching theirs. In addition, the ESP can be considered as a vertically distributed reinforcement. Only the tension reinforcement and the steel plate within a certain area of the tension zone are taken into account when calculating the bearing capacity of the CSW. The area is the distance (h_w-1.5x) to the edge of tension zone, where hw is the total height of the cross-section and x is the height of the compression zone of concrete. The reinforcement and the steel plate that are near the neutral axis are neglected because the reinforcement has little stress, and the steel plate has small area. The vertically distributed reinforcement is not considered in the compression zone due to its small sectional area and susceptibility to buckling. However, the compressive stress of the steel plate, which is restrained by outer concrete on both sides, is considered by assuming that no bucking occurs before the plate yields. The reinforcement deployed in the side column under compression and steel plate yield due to the compression. The basic assumptions in the calculation of the bearing capacity of CSW are:

- The cross-section is planar and the tensile action of concrete within the tension zone is negligible.
- The stress-strain curve of the compression concrete is determined according to the current design code for concrete structures, i.e., a parabola line with $\varepsilon_c < 0.002$, and a horizontal line with $0.002 \le \varepsilon_c < 0.0033$. The ultimate compressive strain of concrete is 0.0033 and the standard compressive strength of concrete f_{ck} is the maximum compressive stress.
- The reinforcement exhibits a linear elastic stress-strain relationship before yielding, while the yield strength is the post-yield stress.

The following equations are used in the calculation:

$$N = f_y' A_s' + f_a' A_a' - f_y A_s - f_a A_a' - N_{sw} - N_{aw} + N_c \tag{1}$$

$$N\left(e_0 + h_w - \frac{h_w}{2}\right) = f_y' A_s' \left(h_{w0} - a_s'\right) - M_{sw} - M_{aw} + M_c \tag{2}$$

$$N_c = f_c \left(b_c - b_w\right) h_c' + f_c b_w x \tag{3}$$

$$N_{sw} = \left(h_w - 1{,}5x - h_c\right) b_w f_{yw} \rho_w \tag{4}$$

$$N_{aw} = \left(h_w - 1{,}5x - h_c\right) t f_{aw} \tag{5}$$

$$M_c = f_c b_c' h_c' \left(h_{w0} - \frac{h_c}{2}\right) + f_c b_w \left(x - h_c'\right)\left(h_{w0} - \frac{h_c}{2} - \frac{x}{2}\right) \tag{6}$$

$$M_{sw} = \frac{1}{2}\left(h_w - 1{,}5x - h_c\right)^2 b_w f_{yw} \rho_w \tag{7}$$

$$M_{aw} = \frac{1}{2}\left(h_w - 1{,}5x - h_c\right)^2 t f_{aw} \tag{8}$$

where x is the height of compression zone in the wall; f_{yw} is the tensile strength of vertical reinforcement distributed in the wall; f_y and f_y' are the tensile and compressive strengths of the longitudinal reinforcement in side columns, respectively; f_a and f_a' are the tensile and compressive strengths of steel in side columns, respectively; A_s and A_s' are the total areas of the longitudinal tension and compression reinforcement in concealed side columns,

Table 5. Comparison of measured and calculated bearing capacities

Specimen	Measured bearing capacity [kN]	Calculated bearing capacity [kN]	Relative error [%]
SPSW-1	706.48	695.75	-1.52
SPSW-2	782.18	745.31	-4.71
SPSW-3	772.54	795.41	2.96
SPSW-4	763.20	739.61	-3.09
RCSW-5	416.06	411.17	-1.18

respectively; A_a and A_a' are the total areas of the tension and compression steel in side columns, respectively; f_c is the compressive strength of concrete; N is the axial force; h_w and b_w are the total height of the cross-section and thickness of the wall, respectively; h_c and h_c' are the heights of the cross-sections of tension and compression side columns, respectively; e_0 is the eccentricity; a_s and a_s' are the distance from resultant points of the longitudinal tension and compression reinforcement in the side columns to the adjacent edge of the cross-section, respectively; h_{w0} is the distance from the outer edge of one side of the shear wall to the central axis of the column on the other side; and ρ_w is the reinforcement ratio of the vertical reinforcement distributed in the shear wall.
The horizontal bearing capacity of a specimen is calculated as follows:

$$F = Ne_0 / H \tag{9}$$

$$e_0 = M / N \tag{10}$$

where, H is the distance from the horizontal loading point to the top of the base of the model.

Using the measured strength of the reinforcement and the concrete, Table 5 shows the calculated maximum bearing capacities for the five specimens. Comparison of calculated and measured bearing capacity values shows that they are close to each other (Table 5).

5. Conclusion

The CSWs with the SRCF and the ESP have higher bearing capacity, better ductility, lower degradation of stiffness, higher energy dissipation capacity, and more significant seismic behaviour as compared to the ordinary reinforced-concrete shear walls. Although the seismic behaviour of CSWs with the SRCF and the ESP is not proportional to the ESP thickness, it can be improved with an appropriate ESP thickness. With the same ESP thickness, the specimens using steel ties exhibit a better seismic behaviour than those using welding studs. Based on the experimental results, a model that can calculate the bearing capacity of CSWs with the SRCF and the ESP was developed. A comparison of the calculated and measured bearing capacities show that they are close to each other. The calculated bearing capacities also have a high safety margin.

Acknowledgements

This research was supported by the Scientific Research Fund of the Institute of Engineering Mechanics, China Earthquake Administration (Grant No. 2016B10), Science and Technology Research Youth Fund for Colleges and Universities in Hebei Province (QN2019076), and the Scientific Research Starting Fund for Postdoctoral Researchers in Heilongjiang Province (Grant No.LBH-Q15146). This support is highly appreciated. Zhongyi Zhou performed the experiments and analysed the data. Wanlin Cao proposed the topic of this study and designed the experiments. Yan Liu analysed the data of the experiments. Jianhua Li performed the experiments and wrote the paper.

REFERENCES

[1] Driver, R.G., Kulak, G.L., Kennedy, D.L., Elwi, A.E.: Cyclic test of four-story steel plate shear wall, Journal of Structural Engineering, 124 (1998) 2, pp. 112-120.

[2] Zhao, Q., Astaneh-Asl, A.: Cyclic behaviour of traditional and innovative composite shear walls, Journal of Structural Engineering, 130 (2004) 2, pp. 271-284.

[3] Rahai, A., Hatami, F.: Evaluation of composite shear wall behaviour under cyclic loadings, Journal of constructional steel research, 65 (2009) 7, pp. 1528-1537.

[4] Hossain, K.M.A., Wright, H.D.: Performance of double skin-profiled composite shear walls - experiments and design equations, Canadian Journal of civil engineering, 31 (2004) 2, pp. 204-217.

[5] Chen, S.J., Jhang, C.: Experimental study of low-yield-point steel plate shear wall under in-plane load, Journal of Constructional Steel Research, 67 (2011) 6, pp. 977-985.

[6] Elgaaly, M., Caccese, V., Du, C.: Postbuckling behaviour of steel-plate shear walls under cyclic loads, Journal of Structural Engineering, 119 (1993) 2, pp. 588-605.

[7] Tsai, K.C., Lin, Y.C., Lin, C.H.: Seismic responses and design of steel plate shear wall, Progress in Steel Building Structures, 9 (2007) 5, pp. 19-25.

[8] Guo, Y., Zhou, M., Dong, Q., Wang, X.: Experimental study on three types of steel plate shear walls under cyclic loading, Journal of Building Structures, 32 (2011) 1, pp. 17-29.

[9] Lu, X., Gan, C., Wang, W.: Study on seismic behaviour of steel plate reinforced concrete shear walls, Journal of Building Structures, 5 (2009), pp. 013.

[10] Sun, J.C., Xu, P.F., Xiao, C.Z., Sun, H.Z., Wang, C.K.: Experimental study on shear behaviour of steel plate-concrete composite wall, Building Structure, 6 (2008), Paper 002.

[11] Jiang, D.Q., Xiao, C.Z., Chen, T., Xu, P.F.: Experimental study of the compression-bending behaviour of highstrength concrete steel composite shear walls, China Civil Engineering Journal, 45 (2012) 3, pp. 17-25.

[12] Zhang, W.J., Cao, W.L., Dong, H.Y., Zhang J.W.: Performance of co-work between steel plate with studs and outer reinforced concrete in shear wall, Journal of Beijing University of Technology, 38 (2012) 6, pp. 828-834.

[13] Cao, W.L., Wang, Y., Dong, H.Y., Zhang, W.J.: Shaking table test study on shear walls with concrete-filled steel tube columns and embedded steel-plate, Earthquake Engineering and Engineering Vibration, 31 (2011) 2, pp. 75-81.

[14] Cao, W.L., Li, G., Zhang, J.W., Zhang, W.J., Geng, H.X.: Seismic behaviour of steel-plate shear walls with concrete filled steel tube columns and different ratio of height to sectional thickness of the walls, Journal of Beijing university of technology, 36 (2010) 8, pp. 1059-1068.

[15] Zhang, J.W., Cao, W.L., Dong, H.Y., Li, G., Zhang, W.J.: Experimental study on seismic performance of steel-plate shear walls with concrete filled steel tube columns and different constructional measures, Journal of Disaster Prevention and Mitigation Engineering, 31 (2011) 4, pp. 450-456.

[16] Zhang, W.J., Cao, W.L., Dong, H.Y., Zhang, J.W., Xu, F.F.: Seismic test and analysis of embedded steel plate concrete shear walls in the exterior bay of a concrete filled square steel tube column frame, Structural engineers, 29 (2013) 1, pp. 130-135.

[17] Tian, S.M.: Rsearch on design method of shear studs in steel plate-concrete shear walls, Building Structure, 6 (2016), pp. 61-66+84.

[18] Code for design of composite structures. JGJ 138 - 2016, Ministry of Housing and Urban-Rural Development, PRC.